Thermal conductivity enhancement of carbon@ carbon nanotube arrays and bonded carbon nanotube network

Materials Research Express

PAPER

Thermal conductivity enhancement of carbon@ carbon nanotube arrays and bonded carbon nanotube network

Majid Kabiri Samani[1,8], **Congxiang Lu**[2,3], **Kong Qinyu**[2], **Narjes Khosravian**[4], **George Chen**[5], **Chong Wei Tan**[2], **Per Rudquist**[1], **Beng Kang Tay**[2,6] and **Johan Liu**[1,7,8]

[1] Electronics Materials and Systems Laboratory (EMSL), Department of Microtechnology and Nanoscience (MC2), Chalmers University of Technology, Kemivägen 9, SE-412 96 Göteborg, Sweden
[2] Center for Micro/Nano-electronics (NOVITAS), School of Electrical and Electronic Engineering, Nanyang Technological University, 639798, Singapore
[3] Ningbo Cataglyphis Intelligent Technology Co., Ltd, Ningbo Hi-Tech Park, Zhejiang 315000, People's Republic of China
[4] Department of Physics, Chalmers University of Technology, Kemivägen 10, 412 96 Gothenburg, Sweden
[5] BC Photonics Technological Co., Richmond, BC V7E 1G9, Canada
[6] CINTRA, CNRS International NTU THALES Research Alliance, Research Techno Plaza, 50 Nanyang Drive, Border X Block, Level 6, 637553, Singapore
[7] SMIT Center, School of Mechanical Engineering and Automation, Shanghai University, No 20, Chengzhong Road, 201800, People's Republic of China
[8] Authors to whom any correspondence should be addressed.

E-mail: kabiri@chalmers.se **and** johan.liu@chalmers.se

OPEN ACCESS

RECEIVED
22 January 2019

REVISED
9 April 2019

ACCEPTED FOR PUBLICATION
1 May 2019

PUBLISHED
17 May 2019

Keywords: CNT array, 3D CNT network, thermal conductivity, thermal interface materials

Supplementary material for this article is available online

Abstract

Carbon nanotubes (CNTs) are long considered as a promising material for thermal applications. However, problems such as low volume CNT fraction abhorrent to practical applications have been raising the demand for novel architecture of this material. Here we demonstrate two fabrication methods, in which a self-assembly method for fabricating covalent-bonded CNT network (3D CNT) and another method for covalent-bonded C to CNTs (C@CNT) network, and presented both as a potential method to enhance thermal conductivity of CNT arrays. We utilized pulsed photothermal reflectance technique and using new four-layer heat conduction model based on the transmission-line theory to measure thermal conductivity of the samples. The 3D CNT with thermal conductivity of 21 W mK^{-1} and C@CNT with thermal conductivity of 26 W mK^{-1} turn out to be an excellent candidate for thermal interface material as the thermal conductivity increased by 40% and 70% respectively as compared to conventional CNT arrays. The improvement is attributed to the efficient thermal routines constructed between CNTs and secondary CNTs in 3D CNT and between C layer and CNTs in C@CNT. The other factor to improve thermal conductivity of the samples is decreasing air volume fraction in CNT arrays. Our fabrication methods provide a simple method but effective way to fabricate 3D CNT and C@CNT and extend the possibility of CNTs towards TIM application.

1. Introduction

Since its discovery of the tubular structure of carbon, carbon nanotube (CNT), has been the focus of research over the years [1]. Individual CNTs have demonstrated excellent electrical, thermal, and mechanical properties, [2–7] and they have been studied for potential applications such as field effect transistors, chemical sensors and scanning probe microscopy components [8–10]. Meanwhile, researchers started to investigate bulk forms of CNTs such as array, bundles, sponges, composite and carpets [11–15]. These bulk forms provide the potential to overcome the difficulties in manipulating a single tube as well as possibility towards applications in a wider range.

One of these applications is to use CNTs as a thermal interface material (TIM). For the past several decades, the performance of integrated circuits (ICs) has improved dramatically because of innovation in process

technologies and continuous increase in density of devices. However, significantly increased device density is also pushing up the requirement to manage high density of heat generated. Actually, successful thermal management has become one of the key factors for long-term reliability of ICs. For even higher device density in the future, it is necessary to further reduce the thermal resistance between the ICs and heat sinks. Currently, TIMs between the IC die and the heat sink has become the bottleneck [16–19]. On one hand, relatively high thermal resistance hinders the heat transport from IC die to the heat sink and becomes an obstacle in the heat dissipating routines. As such, alternative high-performance materials for current TIMs have become a popular research topic.

Among the candidates under investigation, CNT is expected to be a promising solution [12, 18]. More importantly, the extraordinary high thermal conductivity demonstrated by individual CNT provides credit for reduced thermal resistance. However, current CNT based TIM still requires much improvement in the performance. For vertically aligned CNT array, the problem is the limited contact area at the interface, and some short CNTs in the array are not in contact to the other layer. Another problem is low density (low volume fraction of CNTs) of the CNTs in the CNT array. One solution to overcome this problem is to fabricate CNT carpet; however, the thermal performance of the CNT carpet with high density packed of CNT is still far from ideal. This is due to a common problem that CNTs in those bulk forms usually undergo a huge reduction in the extraordinary properties demonstrated by individual tubes [20]. One of the most important reasons is that in those structures, CNTs are stacking together in physical contact with Van der Waals force between them. Electron or phonon propagate between the tubes tends to happen through tunneling effect. Hence, dramatic degeneration of the properties will occur, as inter-tube scattering becomes the dominating factor and overwhelms the properties of single tubes.

In order to overcome these problems, bonded 3D CNT networks is proposed very recently, [21, 22] in which carbon bonds are constructed between CNTs to minimize the inter-tube scattering. The other method is to fabricate the CNT composite without destroying the vertically aligned structure of the CNTs by physical vapor deposition technique. Through depositing metals or carbon around and on top of the CNTs, the air volume fraction in CNT array decreases and by fabricating the metal or carbon layer on top of the CNT arrays, all the CNTs with different length are connected to this layer and contact boundary resistance between the CNT and the deposition layer decreases as well.

In this paper, first, we demonstrate a self-assembly method to fabricate bonded CNT networks and the second we present the method to deposit carbon on the CNTs and investigate thermal properties of the samples. In detail, in the first method, two growth approaches are combined together to fabricate secondary CNTs on vertical CNTs, forming the 3D network of the CNTs and in the second method, high energy carbon ions are deposited around and on top of the CNTs by using the Arc deposition technique. Then, thermal conductivity of the samples are measured by Pulse Photothermal Reflectance (PPR) technique and in order to extract thermal conductivity of the sample by PPR, we developed new four-layer heat conduction model based on the transmission-line theory of heat conduction. With increased contact area at the interface and lower air volume fraction as well as the efficient thermal pathway constructed through carbon bond, the thermal resistance of TIM is reduced significantly.

2. Experiment and samples preparation

2.1. Vertical CNT growth

A nickel film with thickness of 15 nm was deposited on Si wafer through electron beam evaporation as the catalyst (Auto 306, HHV system). Vertical CNTs were fabricated using Aixtron Black Magic plasma enhanced chemical vapor deposition (PECVD) system. The chamber pressure was kept at 10 mPa, with 100 sccm C_2H_2 and 690 sccm NH_3 as the process gases. Growth was carried out at 800 °C for 10 min. The plasma energy was set to 85 watts to accelerate the dissociation of gaseous carbon feedstock, C_2H_2, while a radio frequency (RF) electric field was applied to align the CNTs into a vertical array. Figure 4(a) shows the cross section scanning electron microscopy (SEM) image of the vertical CNT and the tube length is around 7 μm.

2.2. Secondary CNT growth

For the growth of secondary CNTs, nickel nitrate ($Ni(NO_3)_2$) was dissolved in acetone at a concentration of 0.01 M, as the catalyst precursor. The catalyst precursor was cast onto the vertical CNT array at a dose of 10 μl per 1 cm^2. The growth was carried out inside a homemade tube furnace. The furnace pressure was kept at atmospheric pressure during growth. Temperature was ramped up to 700 °C first, under 70 sccm H_2 and 200 sccm Ar atmosphere. When temperature reached 700 °C, ethanol vapor was introduced into the furnace through a bubbler as the carbon source. Growth process took 15 min at 700 °C, after which the ethanol vapor is cut off and samples were then cooled down to room temperature. Figures 4 (a) and (b) show the first growing

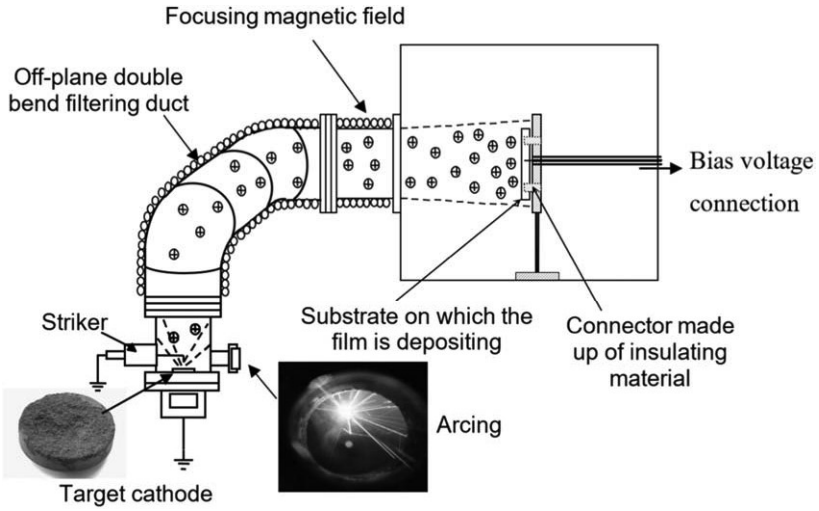

Figure 1. Schematics of Filtered Cathodic Vacuum Arc (FCVA) system.

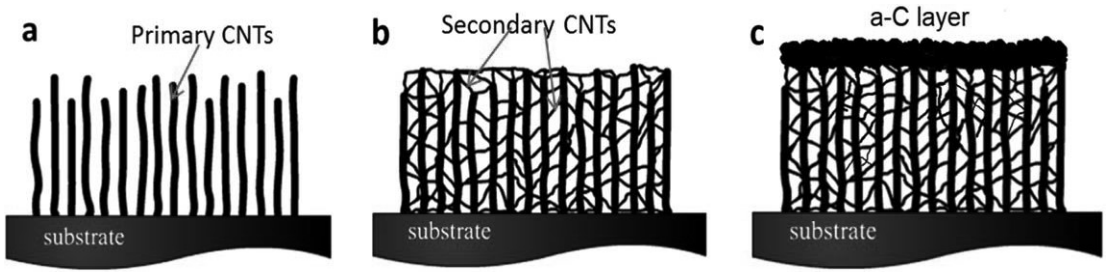

Figure 2. Illustration of the growth procedure. (a) Vertical CNT obtained from PECVD. (b) Formation of 3D CNT network. (c) Deposition of a-C layer on the 3D CNT network.

vertically aligned CNT film by PECVD on Si substrate as explained in sections 2.1 and 3D CNT sample, respectively.

2.3. Carbon deposition on CNTs and 3D CNT

In order to deposit Carbon on the 3D CNT and CNTs, samples were placed in a filtered cathodic vacuum are (FCVA) deposition system. A schematic of the FCVA deposition system is shown in figure 1 and the detail of deposition can be found in the supplementary file. This system is a well-known method to deposit high energy metal and carbon ions on substrates [23]. To accelerate carbon ions and to confine the coating around and on top of the 3D CNT and CNT arrays, a negative pulse bias was used.

As shown in figure 2 and figure 6(b), C ions were deposited on tip of CNTs and secondary CNTs and forms a layer of amorphous carbon (a-C) on top of the 3D CNT network. In this case, carbon ions mainly were absorbed on top of the 3D CNT network because of existing of high density of the secondary CNTs on top and applying the negative pulse bias on them.

As shown in figure 3, in the case of deposition of C on the CNT arrays, a-C layer and sphere was formed on the CNTs because of the high-energy positive carbon ions were accelerated to the side wall and tips of the tubes. As deposition continues, the nano-spheres on the tips of the CNTs increased in size rapidly because of the higher charge density on the tips as shown in figure 6(a). The top layers were formed on top of the samples that adhered very well by covalent bond to the tips and side wall of the tubes.

2.4. Structure characterization

SEM images were taken in a LEO 1550 Gemini field-emission scanning electron microscope (FESEM). Transmission electron microscopy (TEM), high resolution TEM (HRTEM), scanning TEM (STEM) and energy-dispersive x-ray spectroscopy (EDX) line scan were carried out using Tecnai X-TWIN TEM equipped with EDAX Si (Li) detector. A WITec Raman system with a laser wavelength $\lambda = 532$ nm was used to obtain the Raman spectrum.

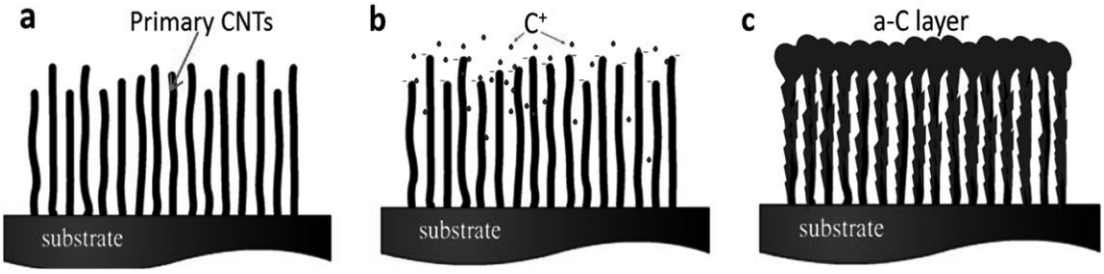

Figure 3. Illustration of the growth procedure. (a) Vertical CNT grown by PECVD. (b) a-C deposition by FCVA system. (c) Formation of a-C layer on and around the CNTs.

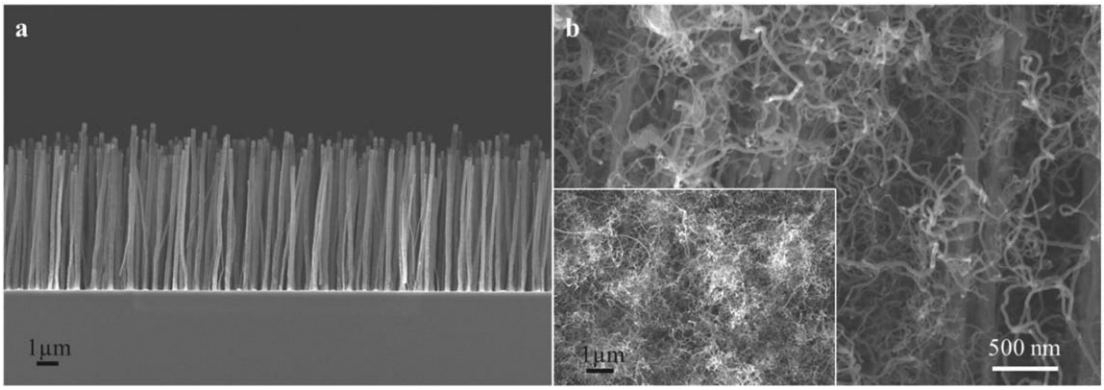

Figure 4. (a) Cross-sectional view of SEM image of the vertical CNT array by PECVD growth. (b) Cross-sectional view of the obtained CNT network after secondary growth process; inset is the top view.

2.5. PPR characterization

PPR technique was employed to investigate the thermal conductivity of the 3D CNT network and C@CNT nano composite. PPR was first used to measure the thermal conductivity of SiO_2 thin film [24], since then it has been widely used to exam the thermal properties of films [25–29]. To enhance the heat absorption, a 250 nm gold layer is evaporated on the surface of the samples. The sample (Au/C layer/CNTs/Si substrate) is first excited by the Nd:YAG laser pulse at the repetition rate of 10 Hz with 3 mm spot size, pulse energy 30.3 mJ and 7 ns pulsed width. This causes a fast rise in the surface temperature and then followed by a relaxation. A 1 mW continuous probe beam (HeNe laser, 632 nm wavelength) with a spot size of about 20 μm is focused on the center of pump beam to monitor the changes in light reflection from the metal surface. Since surface temperature and reflectivity of Au are inversely linearly related [30], the temperature excursion profile in submicrosecond temporal resolution can be obtained by capturing the changes in reflected probe beam. Because the relaxation time is governed by the thermal properties of the underlying layers, by curve fitting the temperature excursion profile with a four-layer one dimensional heat conduction model, one can extract the thermal conductivity of the TIM (3D CNT network or C@CNT layer).

3. Results and analysis

Figure 4(a) is the SEM images of CNTs obtained from PECVD growth. They are well aligned vertically into an array. These CNTs have fairly uniform diameters around 150 nm. The lengths of the CNTs are around 7 μm with slight differences among them. Image processing of several top view SEM images of the CNT array was used to measure surface area fraction of the CNTs and then volume fraction of the CNTs was estimated. The average volume fraction of CNTs is calculated about 10%. After secondary growth process in tube furnace, a network of CNTs is constructed as shown in figure 4(b). It can be seen in the cross-sectional view of SEM image that space in the CNT array is filled up by high density of finer secondary CNTs, which exhibits diameters in the range of 8 to 20 nanometers. Meanwhile in the top view, the sample surface was completely covered by the secondary CNTs. The secondary CNTs have length up to several tens of micrometers and a winding morphology.

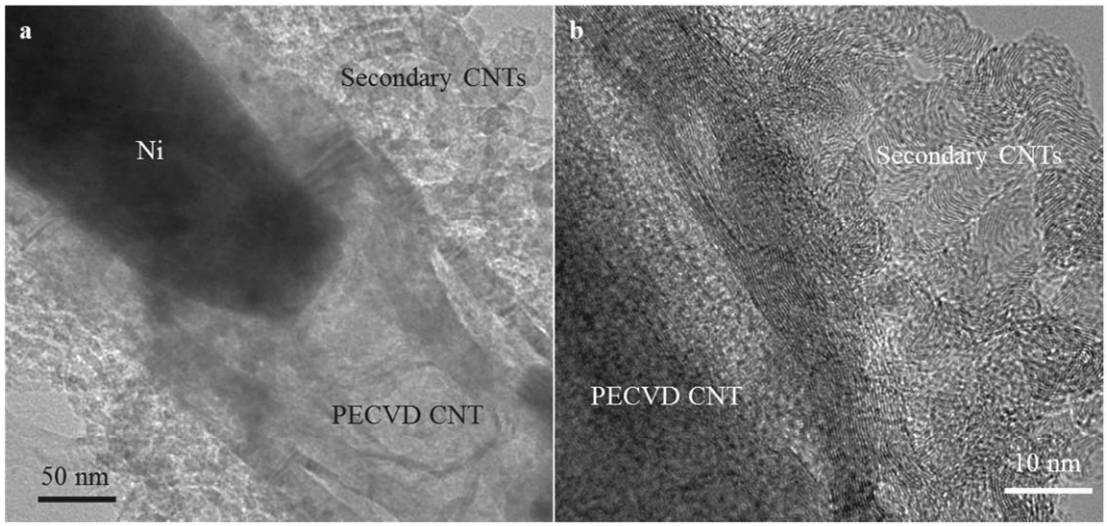

Figure 5. (a) TEM and (b) HRTEM images of the CNT network.

In order to investigate the structure inside the CNTs and also the junctions between CNTs, the obtained 3D CNT network was dispersed in ethanol and examined by TEM. As shown in figure 5, structures of the two hierarchies of CNTs are clearly displayed. CNT with relatively large diameter around 150 nm is the CNT obtained from PECVD, consistent with SEM observation. In this PECVD process, CNTs follow a tip-growth mode. Nickel catalyst particles are lifted up and wrapped in the tip of the CNTs. The bottom part of the nickel particles is the front end of the graphenic formation. As HRTEM has shown clear evidence of the graphitic layers of the carbon nanotube walls with Raman characterization as a supporting information (figure S1, supplementary file is available online at stacks.iop.org/MRX/6/085616/mmedia).

Therefore, there are some graphene sheets left inside CNTs following profile of the bottom part of the nickel particle. This is commonly known as the bamboo structured MWCNTs [31, 32]. On the surface of this CNT, there are a number of CNTs with smaller diameter anchored. These CNTs exhibit a winding morphology and spread all over the surface of CNT. In the HRTEM image figure 5(b), parallel graphitic layers of the tube walls can be seen in both the PECVD and secondary CNTs, which is a signature of the multiwall CNTs. Raman characterization on the samples also shows a typical spectrum of MWCNT [33, 34].

One of the most important concerns in the CNT network is the connection between the CNTs. EDX of the junctions between the CNTs is shown in figure S2 (supplementary file) and provides some evidence. EDX line scan along the junctions shows that only carbon signal can be detected, while signal of other elements are not found. CNTs are bonded together through purely carbon bonds. Hence, the two hierarchies of CNTs are connected into a network rather than randomly packed together without direct bonding in between. It is noted that the bonding is relatively strong, as in the TEM sample preparation, the dispersed sample was under ultrasonic for one hour and the secondary CNTs is still well attached to the surface of primary CNTs.

For the growth of secondary CNTs and formation of the network, the reaction may take place in the following way. During the step of ramping up towards 700 °C, the remaining solvent of the catalyst precursor, acetone, is evaporated. The remaining $Ni(NO_3)_2$ crystallite are left on the surface of primary CNTs. $Ni(NO_3)_2$ can be decomposed and reduced to be nickel particles under Ar/H_2 atmosphere at high temperature.

Here acetone is used because of its relatively low polarity. Due to the high hydrophobicity of CNTs, metal crystallite size is affected significantly by the solvent polarity. Low-polarity acetone will help dispersion of the nickel particles as compared to water or methanol [35]. When ethanol vapor is introduced into the chamber, formation of secondary CNTs is initialized. With the catalyzation effect of nickel particles, ethanol is decomposed to be the carbon feedstock. When the carbon atoms saturate the catalyst particles, they precipitate into a stable tubular structure, which are the secondary CNTs. The secondary CNTs are highly likely to follow a tip growth mode, as evidenced by TEM observations in figure 5, S2 and S3 in supplementary file. The junctions between PECVD and secondary CNTs is purely made of carbon elements and completely free of metal in the EDX line scan, as shown in figure. S2 in supplementary file. Meanwhile, catalyst particles can be found in the tips of some secondary CNTs. As such, it is reasonable to hypothesis that the surface of the CNTs is front-end of secondary CNT formation, after which the nickel catalysts are lift up and located at the tips of the secondary CNTs, eventually.

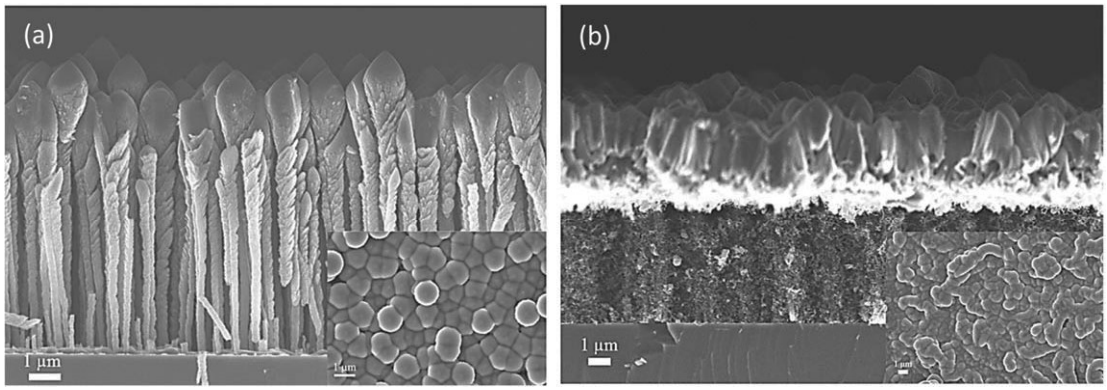

Figure 6. (a) Cross-sectional SEM image of the carbon deposited on PECVD CNT film, inset is the top view (b) Cross- sectional SEM image of the carbon deposited on 3D CNT network, inset is the top view.

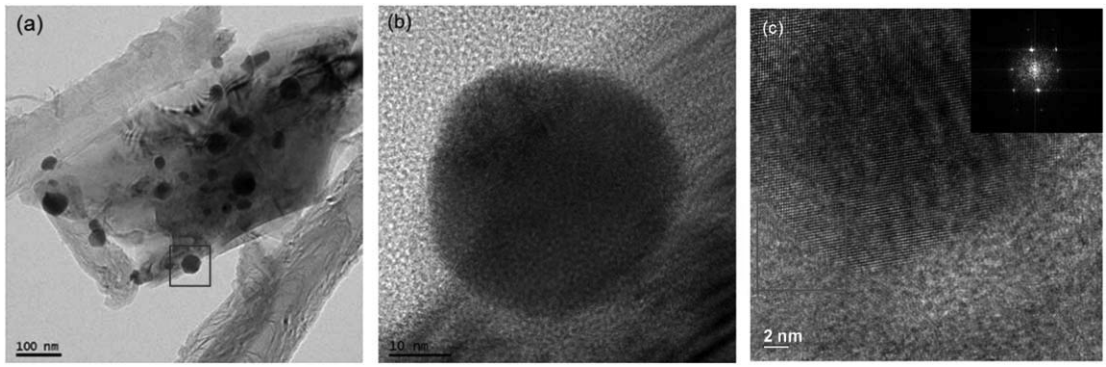

Figure 7. (a) TEM image of the C nanoparticle deposited on the Primary CNT for 10 s deposition time. (b) TEM image of C nanoparticle with higher resoluation. (c) TEM image of the C nanoparticle and SAED pattern.

Figure 6(a) shows the cross-sectional and top view SEM image of the C deposited CNT sample. As it can be seen from the images, the C layer is thicker around the tubes tips and thinner on bottom of the tubes. Most of the C ions were attracted around the tips of CNTs by the electrostatic force because of applying negative bias. Average diameter of the tubes increases from 150 nm to about 300 nm and the air volume fraction decreases from about 90% for CNT array to about 60% for C@CNT accordingly. In the top view, the sample surface was completely covered by the C layer and the diameter of the cones is about 1 μm.

In order to investigate the morphology and microstructure of the contact between the a-C layer and CNTs, a new sample with short carbon deposition time (10 s) was fabricated and TEM analysis was conducted as shown in figure 7. 10 s carbon deposition time was chosen for better visualization of TEM image of carbon nanoparticle and CNT. In the first deposition stage C nanoparticles with diameter around 40 nm were deposited on the side wall of CNTs as shown in figure 7(a) and by continuing the deposition, a-C layer covers the side wall of the CNTs. Figures 7(b) and (c) show the high-resolution images of C nanoparticle deposited on the side wall of CNT. The epitaxy growth of C nanoparticle with respect to the CNT matrix can be seen in the selected area electron diffraction (SAED) pattern in figure 7(c).

3.1. Thermal characterization

The normalized surface temperature profiles for the samples Au/a-C/3DCNT/Si and Au/a-C/C@CNT/Si and their fitted curves are shown in figure 8. To compare experimental data in this study with the primary CNT, we also show the normalized surface temperature of the sample Au foil/CNT/Si in figure 8 as the direct Au deposition on the primary CNT cannot cover the surface of the sample; the Au foil was used to capture photothermal signal. In order to obtain the thermal conductivity of the 3D CNT network and C@CNT layer, the temperature profiles were fitted by a four-layer heat conduction model. In this study, we developed a four-layer heat conduction model based on the transmission-line theory of heat conduction for extracting thermal conductivity of 3D CNT network and C@CNT layers[36]. In this model, the Laplace transformed surface temperature excursions can be expressed by the following equation

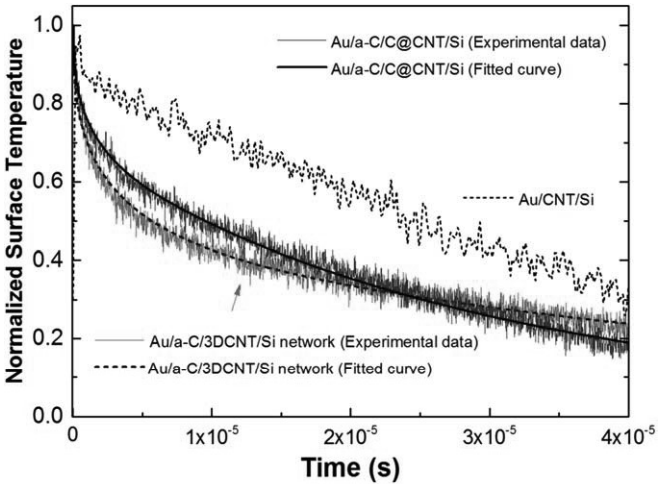

Figure 8. Normalized surface temperature excursion profile of the Au/a-C/3DCNT/Si and Au/a-C/C@CNT/Si samples.

$$T(s) = \mathrm{Q(s)}\left[\frac{Z_1\left(\frac{Z_1 \sinh \eta_1\sqrt{s}}{\cosh \eta_1\sqrt{s}}\right) + \frac{\sigma_1}{e_2\sqrt{s}\,\sigma_2}}{Z_1 + \frac{\sigma_1 \sinh \eta_1\sqrt{s}}{e_2\sqrt{s}\,\sigma_2 \cosh \eta_1\sqrt{s}}}\right] \tag{1}$$

where

$$\sigma_1 = \sinh(\eta_2\sqrt{s})(e_{42}\cosh \eta_3\sqrt{s} + e_{32}\sinh \eta_3\sqrt{s}) + \cosh(\eta_2\sqrt{s})(\cosh \eta_3\sqrt{s} + e_{43}\sinh \eta_3\sqrt{s})$$

$$\sigma_2 = \cosh(\eta_2\sqrt{s})(e_{42}\cosh \eta_3\sqrt{s} + e_{32}\sin h\ \eta_3\sqrt{s}) + \sinh(\eta_2\sqrt{s})(\cos h\ \eta_3\sqrt{s} + e_{43}\sinh \eta_3\sqrt{s})$$

Where $e_i = \sqrt{\rho_i c_i k_i}$, $e_{ij} = e_i/e_j$, $\eta_i = d_i/\sqrt{\alpha_i}$, $Z_1 = 1/(e_1\sqrt{s})$ and i = 1, 2, 3, 4. Subscripts 1, 2, 3 and 4 stand for the Au film, a-C layer, 3D CNT network or C@CNT and Si substrate respectively. *s*, ρ, *c*, *k*, *e*, α, and *d* are the frequency, bulk density, specific heat, thermal conductivity, thermal effusivity, thermal diffusivity, and thickness of each layer respectively. Q(s) is the Laplace transform of the Nd:YAG laser pulse [37]. In order to fit the time domain experimental temperature profile to the theoretical temperature profile, Stehfest numerical method was used to inverse Laplace transform equation (1) into time domain [38]. For the fitting, the least square method was used, in which a function err is defined as the sum of the square of the difference between the experimental temperature profile data and the model's value over the entire measurement time that can be expressed as:

$$err = \sum_{i:\ measurement\ time}(T_{experimental\ data,\ i} - T_{model,\ i}) \tag{2}$$

where $T_{experimental\ data,\ i}$ and $T_{model,\ i}$ are the measured surface temperature and the modeled surface temperature of the Au layer respectively at time t_i. To obtain the best fit, we seek the minimum of err by varying the thermal conductivity of the third layer in the T_{model}.

The obtained room temperature thermal conductivity of 3D CNT film are 21 $\pm$ 5 W mK^{-1}. The result is consistent with earlier reported thermal conductivity of 3D CNT measured by 3-omega method [39]. The average thermal conductivity of the CNT array measured by PPR was previously reported 15 $\pm$ 2 W mK^{-1} [40]. For the 3D CNT network, the thermal conductivity of the sample is increased by about 40%. The thermal conductivity of the 3D CNT network is contributed from the intrinsic thermal conductivity of the CNT, the intrinsic thermal conductivity of secondary CNT and the thermal conductivity of the air gap, $K_{3DCNT} = \gamma_{CNT}K_{int,CNT} + \gamma_{int,\ SecCNT}K_{int,\ SecCNT} + (1 - \gamma_{CNT} - \gamma_{int,\ SecCNT})K_{air}$, where γ is the filling factor of the tubes. The growth of the secondary CNT decreases the air volume fraction and enhances thermal conductivity of the 3D CNT network. The other reason for thermal conductivity enhancement is that, the secondary CNTs work as extra channels to transfer heat at the top surface downward through the CNTs.

For the C@CNT sample, the obtained thermal conductivity is about 26 W mK^{-1} and the improvement on the thermal conductivity is about 70%. After C deposition the diameter of the tubes increases and the air volume fraction decreases to about 60% and based on the equation $K_{C@CNT} = \gamma_{CNT}K_{int,CNT} + \gamma_{C@tube}K_{int,C\ tube} + (1 - \gamma_{CNT} - \gamma_{C@tube})K_{air}$, the thermal conductivity increases. The C layer in this deposition technique adhered very well to the tips and side walls of the CNTs, as the carbon ions formed strong covalent C–C bond and having very low thermal contact resistance between them [41]. The C layer around the CNTs also acts as an extra heat channel to transfer heat to the CNTS and the substrate, thus boosting the array's thermal conductivity.

4. Conclusion

In conclusion, we develop this two-step growth method and successfully fabricate 3D CNT network based on CNT array. More importantly, the secondary CNTs are found to be rooted on surface of the CNTs in array and the two hierarchies of CNTs are connected together by carbon bonds. The other developed sample contains CNTs deposited with C layer on side wall and on top of the CNTs. In these fabrication methods, the air volume fraction is effectively decreased. The thermal conductivity of the samples was measured by PPR technique and four-layer model for the first time was used to extract thermal conductivity. The samples were covered by a-C layer and the layer adhered very well to the CNTs by strong covalent bond with low thermal contact resistance. Much more efficient routines are provided to promote heat propagation from a-C layer to Si substrate. As such, in comparison with thermal conductivity of CNT array TIM, thermal conductivity of the 3D CNT network TIM increased by 40% to be 21 W mK^{-1} which is a significant improvement in the thermal performance. Moreover, thermal conductivity measurement of C@CNT sample shows a higher thermal conductivity about 26 W mK^{-1}, a 70% increment. These methods provide a new approach for the fabrication of 3D CNT network or C@CNT nanocomposite that obtained higher thermal conductivity than CNT array and demonstrated its superiority as high-performance TIM. Moreover, these samples may also be extended to applications in other areas such as chemical filer or mechanical cushion.

Acknowledgments

We thank for the financial support from the Swedish Foundation for Strategic Research (SSF) under contract (No SE13–0061), Swedish National Board for Innovation (Vinnova) Graphene SIO-Agenda Program, Formas program on graphene enhanced composite as well as from the Production Area of Advance at Chalmers University of Technology, Sweden. Thanks are also given to the Ministry of Science and Technology of China with the contract No: 2017YFB040600 for the financial support. This research benefited also from the support of the Ministry of Education (Singapore) under the grand MOE2014-T2-2-105.

ORCID iDs

Chong Wei Tan https://orcid.org/0000-0002-9540-8708
Johan Liu https://orcid.org/0000-0001-9931-1439

References

[1] Iijima S 1991 Helical microtubules of graphitic carbon *Nature* **354** 56–8
[2] Ebbesen T W, Lezec H J, Hiura H, Bennett J W, Ghaemi H F and Thio T 1996 Electrical conductivity of individual carbon nanotubes *Nature* **382** 54–6
[3] Li H J, Lu W G, Li J J, Bai X D and Gu C Z 2005 Multichannel ballistic transport in multiwall carbon nanotubes *Phys. Rev. Lett.* **95** 1–4
[4] Kim P, Shi L, Majumdar A and McEuen P L 2001 Thermal transport measurements of individual multiwalled nanotubes *Phys. Rev. Lett.* **87** 2155021–4
[5] Fujii M, Zhang X, Xie H, Ago H, Takahashi K, Ikuta T, Abe H and Shimizu T 2005 Measuring the thermal conductivity of a single carbon nanotube *Phys. Rev. Lett.* **95** 1–4
[6] Treacy M M J, Ebbesen T W and Gibson J M 1996 Exceptionally high Young's modulus observed for individual carbon nanotubes *Nature* **381** 678–80
[7] Yu M F, Lourie O, Dyer M J, Moloni K, Kelly T F and Ruoff R S 2000 Strength and breaking mechanism of multiwalled carbon nanotubes under tensile load *Science* **287** 637–40
[8] Dai H J, Hafner J H, Rinzler A G, Colbert D T and Smalley R E 1996 Nanotubes as nanoprobes in scanning probe microscopy *Nature* **384** 147–50
[9] Kong J, Franklin N R, Zhou C W, Chapline M G, Peng S, Cho K J and Dai H J 2000 Nanotube molecular wires as chemical sensors *Science* **287** 622–5
[10] Tans S J, Verschueren A R M and Dekker C 1998 Room-temperature transistor based on a single carbon nanotube *Nature* **393** 49–52
[11] Chen H, Chen M, Di J, Xu G, Li H and Li Q 2012 Architecting three-dimensional networks in carbon nanotube Buckypapers for thermal interface materials *J. Phys. Chem.* C **116** 3903–3909
[12] Cola B A, Xu J and Fisher T S 2009 Contact mechanics and thermal conductance of carbon nanotube array interfaces *Int. J. Heat Mass Transfer* **52** 3490–503
[13] Zhang K, Chai Y, Yuen M M F, Xiao D G W and Chan P C H 2008 Carbon nanotube thermal interface material for high-brightness light-emitting-diode cooling *Nanotechnology* **19** 21
[14] Gui X C, Wei J Q, Wang K L, Cao A Y, Zhu H W, Jia Y, Shu Q K and Wu D H 2010 Carbon nanotube sponges *Adv. Mater.* **22** 617–61
[15] Pradhan N R, Duan H, Liang J and Iannacchione G S 2009 The specific heat and effective thermal conductivity of composites containing single-wall and multi-wall carbon nanotubes *Nanotechnology* **20** 245705
[16] Schelling P K, Shi L and Goodson K E 2005 Managing heat for electronics *Mater. Today* **8** 30–5
[17] Sarvar F, Whalley D C and Conway P P 2006 Thermal interface materials - A Review of the State of the Art *1st Electronic Systemintegration Technology Conference* Vol. 2 (New York: IEEE) pp. 1292–302

[18] Xu J and Fisher T S 2006 Enhanced thermal contact conductance using carbon nanotube array interfaces *IEEE Trans. Compon. Packag. Technol.* **29** 261–7
[19] 2009 International Technology Roadmap for Semiconductors 4
[20] Berber S, Kwon Y K and Tománek D 2000 Unusually high thermal conductivity of carbon nanotubes *Phys. Rev. Lett.* **84** 4613–6
[21] Hashim D P *et al* 2012 Covalently bonded three-dimensional carbon nanotube solids via boron induced nanojunctions *Sci. Rep.* **2**
[22] Fu Y *et al* 2012 Templated growth of covalently bonded three-dimensional carbon nanotube networks originated from graphene *Adv. Mater.* **24** 1576–81
[23] Sheeja D, Tay B K, Sze J Y, Yu L J and Lau S P 2003 A comparative study between pure and Al-containing amorphous carbon films prepared by FCVA technique together with high substrate pulse biasing *Diamond Relat. Mater.* **12** 2032–6
[24] Kading O W, Skurk H and Goodson K E 1994 Thermal conduction in metallized silicon-dioxide layers on silicon *Appl. Phys. Lett.* **65** 1629–31
[25] Zhao Y M, Chen G, Wang S Z and Yoon S F 2004 Thermal characterization of gallium arsenic nitride epilayer on gallium arsenide substrate using pulsed photothermal reflectance technique *Thin Solid Films* **450** 352–6
[26] Panzer M A, Duong H M, Okawa J, Shiomi J, Wardle B L, Maruyama S and Goodson K E 2010 Temperature-Dependent phonon conduction and nanotube engagement in metalized single wall carbon nanotube films *Nano Lett.* **10** 2395–400
[27] Samani M K, Ding X Z, Khosravian N, Amin-Ahmadi B, Yi Y, Chen G, Neyts E C, Bogaerts A and Tay B K 2015 Thermal conductivity of titanium nitride/titanium aluminum nitride multilayer coatings deposited by lateral rotating cathode arc *Thin Solid Films* **578** 133–8
[28] Jing L, Samani M K, Liu B, Li H, Tay R Y, Tsang S H, Cometto O, Nylander A, Liu J and Teo E H T 2017 Thermal conductivity enhancement of coaxial carbon@ boron nitride nanotube arrays *ACS Applied Materials & Interfaces* **9** 14555–60
[29] Han H *et al* 2016 Functionalization mediates heat transport in graphene nanoflakes *Nat. Commun.* **7** 11281
[30] Ujihara K 1972 Reflectivity of metals at high temperatures *J. Appl. Phys.* **453** 2376–83
[31] Cui H, Zhou O and Stoner B R 2000 Deposition of aligned bamboo-like carbon nanotubes via microwave plasma enhanced chemical vapor deposition *J. Appl. Phys.* **88** 6072–4
[32] Delzeit L, McAninch I, Cruden B A, Hash D, Chen B, Han J and Meyyappan M 2002 Growth of multiwall carbon nanotubes in an inductively coupled plasma reactor *J. Appl. Phys.* **91** 6027–33
[33] Zhao X, Ando Y, Qin L C, Kataura H, Maniwa Y and Saito R 2002 Radial breathing modes of multiwalled carbon nanotubes *Chem. Phys. Lett.* **361** 169–74
[34] Costa S, Borowiak-Palen E, Kruszyñska M, Bachmatiuk A and Kaleńczuk R J 2008 Characterization of carbon nanotubes by Raman spectroscopy *Materials Science- Poland* **26** 433–41
[35] Azadi P, Farnood R and Meier E 2009 Preparation of multiwalled carbon nanotube-supported nickel catalysts using incipient wetness method† *The Journal of Physical Chemistry* A **114** 3962–8
[36] Chen G and Hui P 1999 Pulsed photothermal modeling of composite samples based on transmission-line theory of heat conduction *Thin Solid Films* **339** 58–67
[37] Ding X-Z, Samani M K and Chen G 2010 Thermal conductivity of PVD TiAlN films using pulsed photothermal reflectance technique *Appl. Phys.* A **101** 573–7
[38] Cheng A H, Sidauruk P and Abousleiman Y 1994 Approximate inversion of the Laplace transform *Mathematica Journal* **4** 76–82
[39] Kong Q, Qiu L, Lim Y D, Tan C W, Liang K, Lu C and Tay B K 2018 Thermal conductivity characterization of three dimensional carbon nanotube network using freestanding sensor-based 3ω technique *Surf. Coat. Technol.* **345** 105–12
[40] Yang D J, Zhang Q, Chen G, Yoon S F, Ahn J, Wang S G, Zhou Q, Wang Q and Li J Q 2002 Thermal conductivity of multiwalled carbon nanotubes *Phys. Rev.* B **66**
[41] Shuangxi S, Kabiri S M, Yifeng F, Tao X, Lilei Y, Maulik S, Kjell J, Torbjörn N, Litao S and Johan L 2018 Improving thermal transport at carbon hybrid interfaces by covalent bonds *Advanced Materials Interfaces* **5** 1800318